Materials Science and Engineering A 523 (2009) 118–124

Contents lists available at ScienceDirect

Materials Science and Engineering A

journal homepage: www.elsevier.com/locate/msea

The response of aluminium/GLARE hybrid materials to impact and to in-plane fatigue

F. Bagnoli[a], M. Bernabei[a], D. Figueroa-Gordon[b], P.E. Irving[b,*]

[a] Flight Test Centre, Chemistry Department, Pratica di Mare Airport, 00040 Pomezia (Rome) Italy
[b] Department of Materials Cranfield University, Cranfield, MK43 0AL, United Kingdom

ARTICLE INFO

Article history:
Received 4 February 2009
Received in revised form 19 May 2009
Accepted 27 May 2009

Keywords:
Bonded hybrids
Damage tolerance
Fatigue crack growth
Fibre metal laminates
Impact

ABSTRACT

Fibre metal laminates (FMLs), such as glass reinforced aluminium (GLARE), are a family of materials with excellent damage tolerance and impact resistance properties. This paper presents an evaluation of the low velocity impact behaviour and the post-impact fatigue behaviour of GLARE laminate adhesively bonded to a high strength aluminium alloy substrate as a fatigue crack retarder. The damage initiation, damage progression and failure modes under impact and fatigue loading were examined and characterised using an ultrasonic phased array C-scan together with metallography and scanning electron microscopy (SEM). After impact on the substrate, internal damage to the GLARE bonded on the opposite side of the substrate occurred in the form of fibre and matrix cracking. No delamination was detected at the GLARE/substrate bond. Before impact the bonded GLARE strap caused reductions in substrate fatigue crack growth rate of up to a factor of 5. After impact the retardation was a factor of 2. The results are discussed in terms of changes to the GLARE stiffness promoted by the impact damage.

1. Introduction

In the last decades both civil and military aircraft have been operated at service lives well beyond their original design life. Due to military budgetary constraints and civilian industry requirements, all of these older aircraft either have encountered ageing problems, such as fatigue cracking, stress corrosion cracking (SCC) or corrosion [1,2]. Fatigue cracks often initiate from impact damage occurring during pre-flight and taxiing operations, dropped tools during maintenance, runaway debris, hail or bird strike [3,4]. Such damaged structures are frequently required to remain in service for extended periods, despite the occurrence of damage. In design of new aircraft structures, lower density and higher operational stress levels are often required to achieve the desired weight. Use of welding [5] can give economy of construction. However, both use of high strength materials and of integral welded structures make achievement of fail safety and damage tolerance difficult. Regulators can penalise such structures by imposition of extra design safety factors. Airworthiness regulations require the damage tolerance and fail safe philosophy to be adopted [6,7]. For such reasons, the use of crack retarder devices to stop or limit fatigue crack growth is a possibility to improve fail safety and damage tolerance. In aircraft repair, mechanically fastened metallic reinforcements with either bolts or rivets have been used successfully for many years. However, they introduce additional stress concentrations into the damaged area. Holes must be drilled for mechanical fasteners and may also damage internal components during the repair. Use of bonded repairs and crack retardation methods may be the easiest and cheapest solution to overcome these problems. Use of adhesively bonded repair with either metal or composites patches on 2024-T3 has received a lot of attention [8,9]. Disadvantages include material compatibility problems. Boron/epoxy and carbon/epoxy have lower coefficient of thermal expansion (CTE) than aluminium, thus causing residual stresses in the repair. Moreover, the presence of graphite could create galvanic corrosion problems. As a consequence of these problems, other patch materials, such as titanium or fibre-metal laminates (FML) such as GLARE have been investigated, showing their effectiveness in retarding or arresting the crack [10,11]. FMLs combine good fatigue performance with the excellent impact resistance [2,12–20]. The use of FMLs as crack retarders may help to improve the damage tolerance of structures and a number of recent papers have demonstrated the benefits of following this approach, e.g. [21]. Schijve [22] showed that thin straps of aramid reinforced aluminium laminate (ARALL) bonded to aluminium panels are effective as crack stoppers in thin structures. The effect of the crack retarder on crack growth rate could be quantified using the global stiffness ratio μ, defined as:

$$\mu = \frac{\sum(E_{\text{Strap}}A_{\text{Strap}})}{(E_{\text{Al}}A_{\text{Al}}) + \sum(E_{\text{Strap}}A_{\text{Strap}})} \quad (1)$$

* Corresponding author. Tel.: +44 1234 754129; fax: +44 1234 752376.
E-mail address: p.e.irving@cranfield.ac.uk (P.E. Irving).

0921-5093/$ – see front matter © 2009 Elsevier B.V. All rights reserved.
doi:10.1016/j.msea.2009.05.055

Table 1
Tensile properties of the AA7085-T7651 [32].

Orientation	0.2% proof stress (MPa)	Tensile strength (MPa)	Elongation (%)
L	596	612	7.3
LT	413	436	6.9

where E_{Strap}, E_{Al} and A_{Strap}, A_{Al} correspond to the elastic modulus and cross section areas of the strap and aluminium substrate, respectively. Heinimann et al. [23,24] investigated GLARE bonded to AA7085-T7651 plates and showed that crack growth life can be improved by a factor of 2–4. Zhang et al [25–27] noted that in addition to the stiffness ratio μ, the effects of the strap are a function of residual stresses arising in the strap bonding process and out of plane bending caused by the single sided strap application. Although the impact resistance and damage tolerance of FMLs have been extensively investigated over the years, there is limited published work on post-impact fatigue response of bonded retarders [28–31].

The work reported in this paper investigates the effect of impact damage on crack retardation performance of GLARE 1 straps bonded to a 5 mm thick aluminium substrate. The impacts were made to the substrate on the opposite side to the bonded layer. The effects of the impact on damage in the GLARE and in the adhesively bonded layer were determined, along with the post-impact performance of the bonded strap as a crack retarder.

2. Experimental procedure

2.1. Materials and test configurations

The aluminium alloy 7085-T7651 was chosen as the substrate. Table 1 summarises the 7085 tensile strength properties [32]. Fig. 1 shows the substrate microstructure viewed along the three principal directions. The substrate was 5 mm thick. GLARE 1-3/2 was chosen as the crack retarder strap material. GLARE 1-3/2 consists of three layers of 7475-T761 aluminium alloy and two

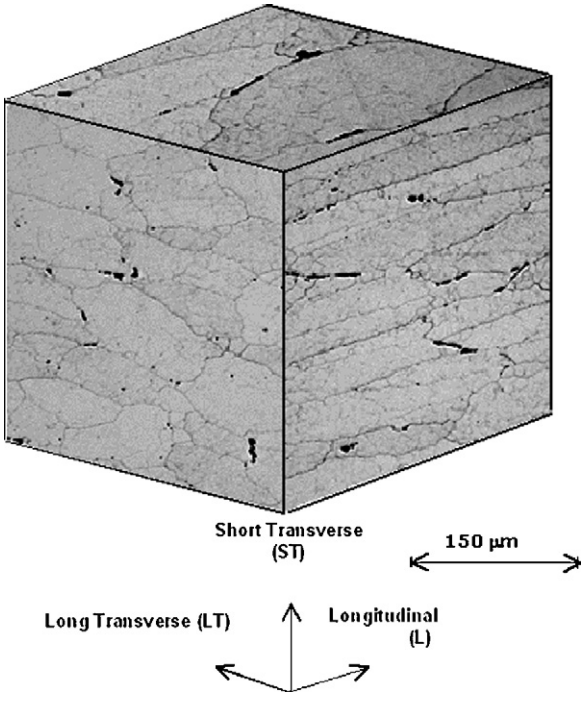

Fig. 1. Microstructure of the wrought AA7085-T7651 alloy viewed along the three principal directions.

Table 2
Tensile properties of the GLARE 1-3/2 tested [31].

Tensile ultimate strength (MPa)	0.2% Tensile yield strength (MPa)	Tensile elastic modulus (GPa)	Tensile ultimate strain (%)
L LT	L LT	L LT	L LT
1.28 352	545 333	65 50	4.2 7.7

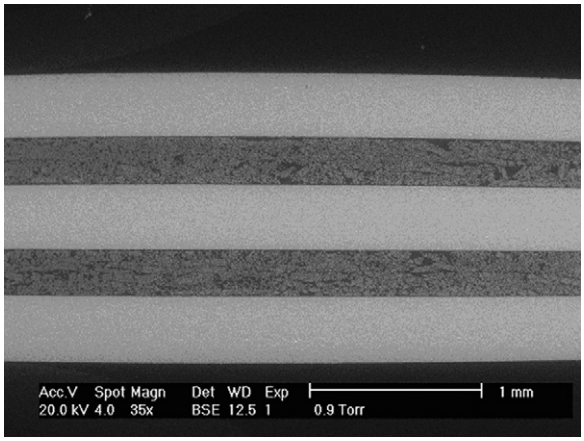

Fig. 2. Transverse cross sectional view of GLARE 1-3/2.

layers of 0°/0° glass reinforced epoxy pre-preg. It was 1.78 mm thick. In Table 2 the tensile properties of the GLARE 3/2 are listed [31]. Fig. 2 shows the transverse cross section view of the GLARE material. FM® 94 modified epoxy adhesive film, supplied by Cytec, was chosen to bond the GLARE to the substrate. This is the same adhesive as used to bond the aluminium and glass fibre layers of the GLARE together. Details of the mechanical performance can be found at [33]. The specimen configurations used for this study are shown in Figs. 3 and 4. For impact tests (Fig. 3) the GLARE (115 mm × 65 mm × 1.78 mm thick) was bonded in the middle of rectangular plates (150 mm × 100 mm × 5 mm thick). For the fatigue crack growth tests (Fig. 4) the straps (200 mm × 25 mm × 1.78 mm thick) were bonded to single edge notch tensile (SENT) aluminium plates (400 mm × 140 mm × 5 mm thick). The edge of the GLARE strap was 20 mm from the notch tip (37 mm from the SENT plate edge). The global stiffness ratio of the fatigue samples as calculated using Eq. (1) was 0.056. The surface of the substrate was etched with a sulphuric acid/sodium dichromate bath held at 60 °C prior to applying the adhesive. The specimens were bonded following manufacturers instructions and cured 1 h at 125 °C. After cure the specimens were inspected using an ultrasonic phased array C-scan to confirm their bond quality prior to impact and fatigue tests. The hot cure process will introduce ten-

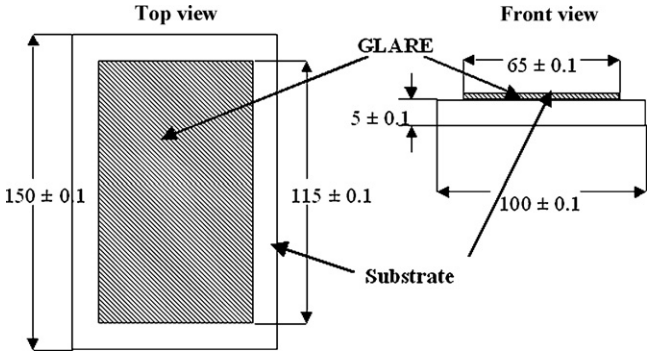

Fig. 3. Impact test sample design specification dimensions expressed in mm.

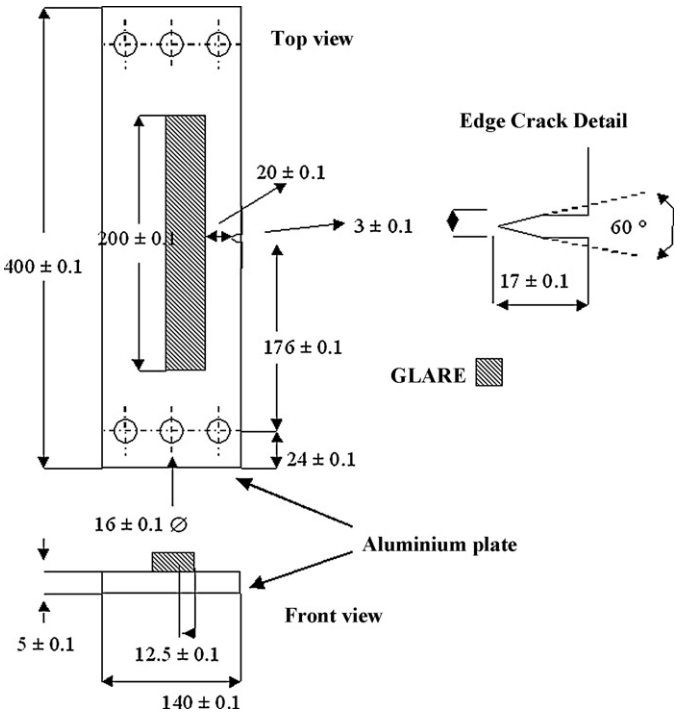

Fig. 4. Fatigue test sample design specification. Dimensions expressed in mm.

sile residual stresses [26] into the substrate; modifying the changes in crack growth rate in all the samples identically.

2.2. Mechanical test methods

Impact tests were performed with an instrumented falling–weight machine fitted with a second strike preventer. The specimens were clamped within a steel frame having a rectangular aperture and struck at the centre of the aluminium substrate by a hemispherical tup 20 mm in diameter. The total mass of the impactor was 2.54 kg. A range of impact energies between 10 and 50 J were achieved by changing the drop height. Four specimens were tested at each energy level. After impact specimens were scanned ultrasonically using a phased array probe located on the substrate side to assess the extent of damage sustained to the interface and to the GLARE. Samples were then sectioned through the mid plane of the impact, polished and finally examined by metallographic microscopy and SEM to observe the damage patterns and failure mechanisms.

Fatigue crack growth tests were performed on a 250 kN servo hydraulic machine equipped with digital control. Specimens were subjected to fatigue loading at 8 Hz and R ratio of 0.1. The starting load range of 46.75 kN, was progressively reduced so that as the crack tip encountered the edge of the strap, the nominal ΔK was 10 MPa $\sqrt{m}$. Once this condition was reached, the loads were kept constant until the tests finished. Two fatigue specimens were impacted before fatigue testing using the procedure previously described. They were struck on the substrate so that an indentation opposite the middle of the strap was produced. A further specimen was tested without prior impact. Fatigue crack growth rates were compared with those produced in a 7085 sample tested without a bonded GLARE strap. Crack lengths were measured using a travelling microscope to calibrate an electrical potential crack length measurement system. The accuracy of crack length measurement was ± 0.2 mm. Delamination damage produced by impacts and by fatigue crack growth was measured using an ultrasonic phased array C-scan applied to the substrate side of the sample. After testing samples were examined in the SEM.

3. Results

3.1. Impact behaviour

The response to the impact is described in terms of force–time curves produced by different impact energies (Fig. 5). Peak forces during impact ranged from 10 kN for 10 J impacts to about 25 kN in the case of the specimens impacted at 50 J. All the curves show pronounced oscillations throughout and, unlike the corresponding curves for polymer matrix composites, do not exhibit any sudden load drops. Each load transient was less than 2 ms in duration. The period of oscillation in each test was 0.2 ms, independent of the impact energy. The maxima and minima of each oscillation occurred at approximately the same time, as indicated by the arrow markers in Fig. 5. The maximum force occurred at the same time after impact (0.8 ms) for all impact energies. Fig. 6 shows a graph of the maximum force obtained from the force–time curves vs. the impact energy. Over the range of energies studied, the trend is linear.

3.1.1. Impact damage visual observations on the external surface

The impact produced an approximately circular indentation on the substrate outer surface (see Fig. 7). On the GLARE side of the sample the external surface developed a local bulge opposite the impact site; it was roughly elliptical shape with the long axis oriented along the glass reinforcement direction. The dent and bulge areas were measured using an optical microscope. Table 3 shows the optically detectable damage areas produced on the substrate

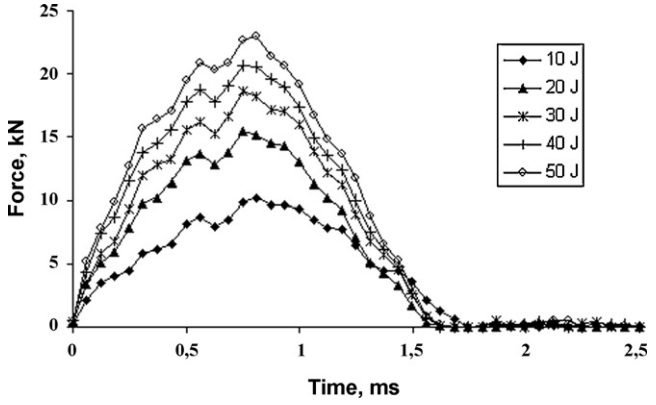

Fig. 5. Force vs. time history of impacts on substrate/ GLARE specimens.

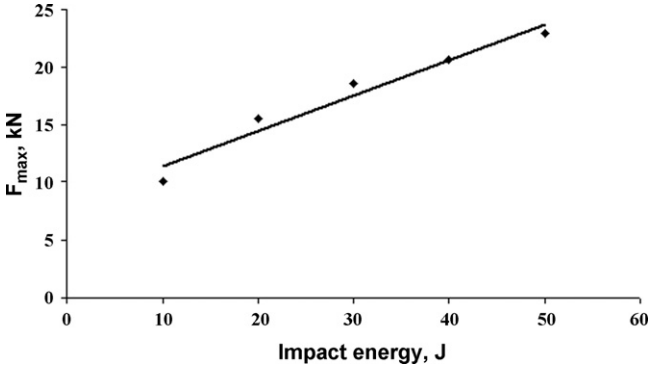

Fig. 6. Maximum force vs. impact energy for impact events on substrate/GLARE specimens.

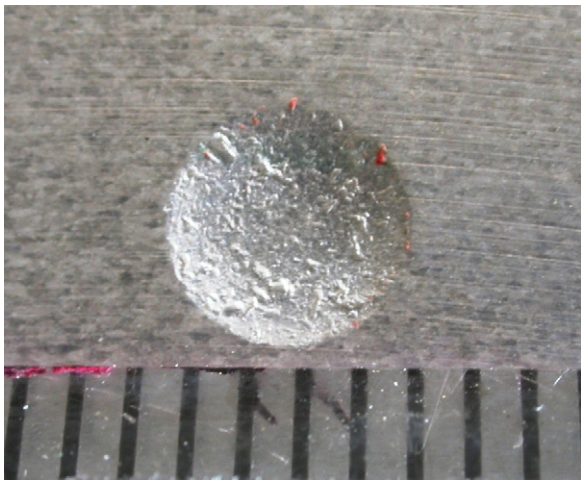

Fig. 7. Indentation produced on substrate after impact at 50 J.

Table 3
Visually detectable dent and bulge areas produced on substrate and GLARE surfaces after impact.

Energy (J)	Indent area on substrate side (mm^2)	Bulge area on GLARE side (mm^2)
10	3.80	None visible
20	6.68	None visible
30	8.04	31.40
40	11.13	61.23
50	15.90	89.94

and on the GLARE sides of the sample. Surface damage on both sides increases with increasing impact energy. For the greatest impact energies, the bulge area produced on the GLARE side is approximately 5 times greater than the dent area on the substrate. C-scan measurements revealed that the damaged areas in GLARE had a roughly elliptical shape as shown in Fig. 8. Fig. 9 shows a plot of the impact damage area as measured using ultrasound and shows that the damage area increases with increasing impact energy, reaching 800 mm^2 after 50 J impact. This is almost a factor of 10 times greater than the damage area visually detectable listed in Table 3.

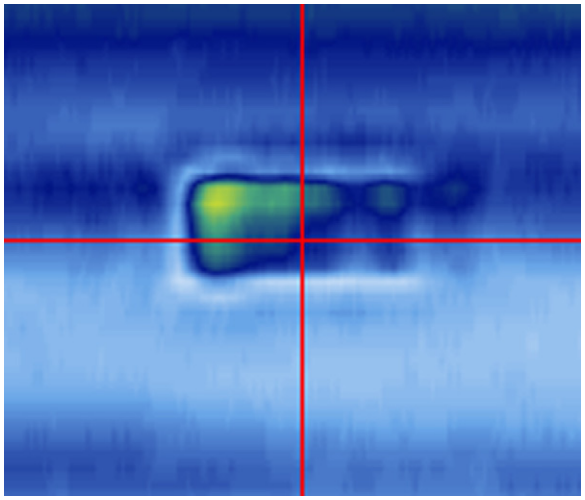

Fig. 8. Phased array C-scan image of delamination damage produced after 30 J impact on to the aluminium substrate.

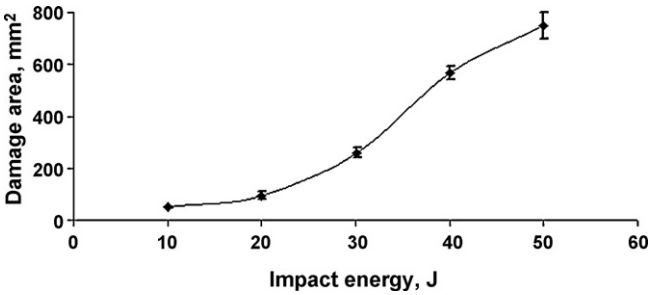

Fig. 9. Damage area in GLARE layer vs. substrate impact energy. The error bars refer to the calculated standard deviation from the 4 samples tested at each energy level.

3.1.2. Impact damage observations on sections through the impacts

For all specimens fibre failure and matrix cracking were found in the two glass layers within the GLARE. Figs. 10 and 11 show examples of fibre fracture and matrix cracking within the glass layer furthest from the substrate. For a 50 J impact, the percentage of fibres cracked was about 60% of the total in the first glass layer, and about 90% in the second layer. Cracks occurred both along and through the fibre. The matrix cracks were not located directly beneath the impact area, but started towards the edges of the damage. Fibre cracking was observed transverse, longitudinal and at 45° with respect to the fibre axis, as shown in Fig. 12. No delaminations were found at the aluminium/epoxy interfaces within the

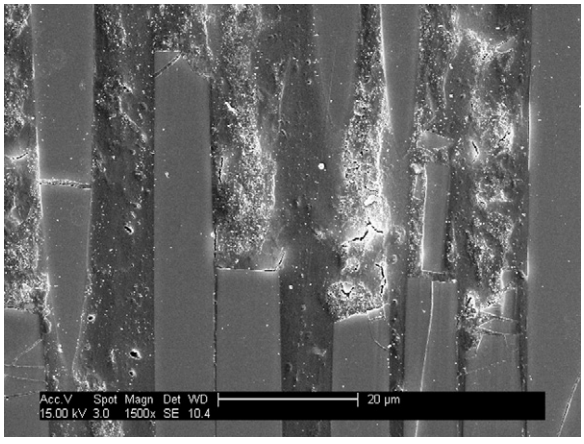

Fig. 10. SEM micrograph showing fibre and matrix cracking in second glass layer within the GLARE after 40 J impact on the substrate.

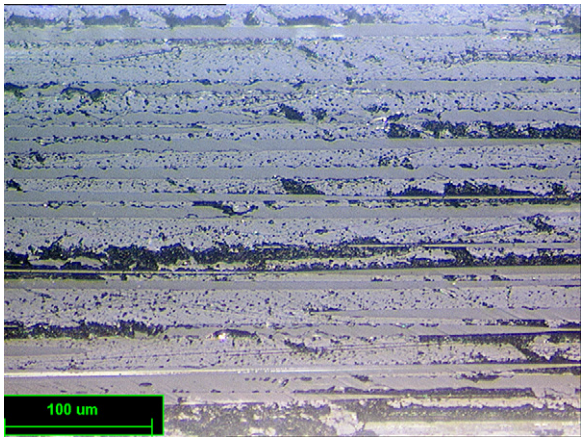

Fig. 11. Optical micrograph showing matrix cracking in the glass layer within the GLARE. Edge of the impact damage zone after 50 J impact on the substrate.

Fig. 12. Optical micrograph showing cracks in the glass fibres at 45° (see arrows) with respect to the fibre axis in second glass layer within GLARE after 50 J impact on the substrate.

GLARE. No delaminations were found at the interface between the substrate and the outer GLARE aluminium layer. All damage appeared to be confined to the glass layers within the GLARE laminate.

3.2. Fatigue crack growth tests

Fig. 13 shows crack growth rates plotted against crack length for a sample with a bonded strap compared with growth rates from the substrate alone. Maximum retardation effect is found at the first strap edge where there is a reduction in growth rate of a factor of 5 for the unimpacted specimen. In addition, there appears to be a reduction in growth rate in the zone before the crack tip had reached the strap edge. While the crack tip was under the strap further reductions in growth rate occurred. As the crack tip passed the second strap edge the growth rates were about a factor of 2 less than those found in the substrate alone. Fig. 14 shows plots of crack length vs. cycles for unimpacted samples and for samples impacted at 10 and 30 J. Before the first strap edge is approached, the behaviour of the samples are similar. Once the strap edge is reached behaviour differences are observed. In particular, the unimpacted specimen shows a longer fatigue life than the impacted specimens. The specimen impacted at 30 J has the shortest crack growth life, with a reduction in fatigue life of about 30.5% compared with the unimpacted one. For the specimen impacted at 10 J the reduction is about 12.5%.

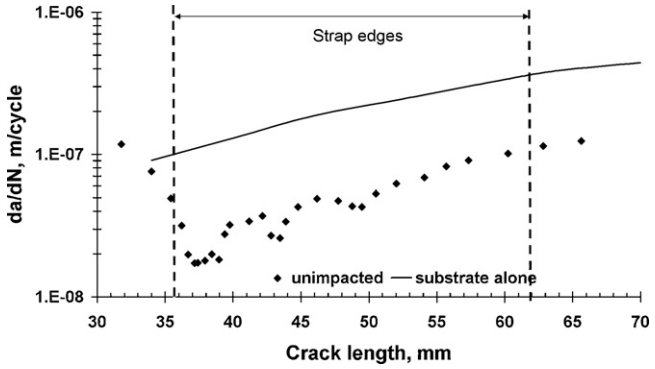

Fig. 13. Changes in fatigue crack growth rate in substrate caused by the retardation action of the strap. Fatigue crack growth rates in 7085 without a bonded strap are also shown for comparison.

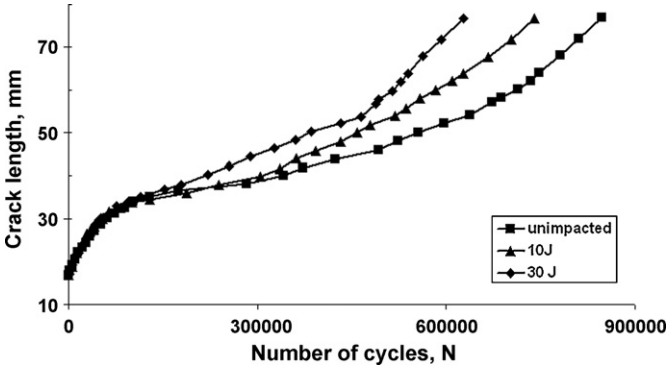

Fig. 14. Fatigue crack length vs. fatigue cycles for crack growth in the substrate across the GLARE strap in unimpacted samples and in ones impacted at 10 J and 30 J.

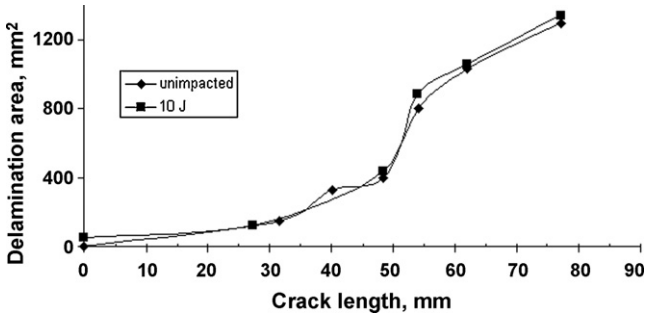

Fig. 15. Delamination development within the GLARE strap caused by the propagation of the substrate fatigue crack.

3.2.1. Delamination development in fatigue

When the substrate fatigue crack encountered the strap edge, it did not propagate through the GLARE but instead promoted a delamination between the outer aluminium lamina bonded to the substrate and the first glass layer within the GLARE. This was observed in all fatigue specimens. The extent of this delamination was measured by ultrasonic phased array C-scan. Fig. 15 shows the increase in delamination area produced as the substrate crack length increases. A small delamination developed as the crack tip approached the strap edge, this increased markedly when the crack tip tunneled under the strap and continued to increase in size as the crack tip moved beyond the strap.

3.2.2. Fracture surface observations

The fatigue fracture surface of the unimpacted specimen is shown in Fig. 16. The substrate fatigue fracture propagated into the first aluminium layer of the GLARE, fracturing that completely. The main delamination propagated between the first aluminium layer and the first grp layer within the GLARE, separating the aluminium from the rest of the GLARE. A subsidiary delamination developed between the substrate and the FM94 adhesive bonding the outer GLARE layer to the substrate. This is visible in Fig. 17.

4. Discussion

4.1. Impact behaviour

Load changes during impacts on polymer composite materials [34] and FMLs [35,36] can be characterised by an initial rise in load to a maximum value of load followed by a sudden sharp drop in the load, indicating the presence of failure, such as a delamination [35] or a puncture related to a full penetration. This point represents the damage initiation threshold force. After puncture the impact energy is not fully recovered as for an elastic event but it is

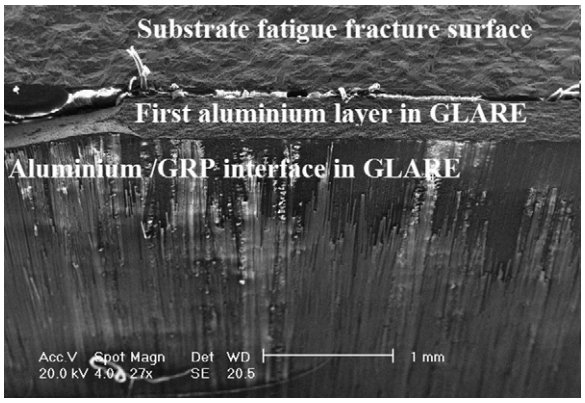

Fig. 16. SEM micrograph showing the fatigue fracture surface in the substrate together with the major delaminated surface in the first glass/aluminium interface within the GLARE. Sample unimpacted.

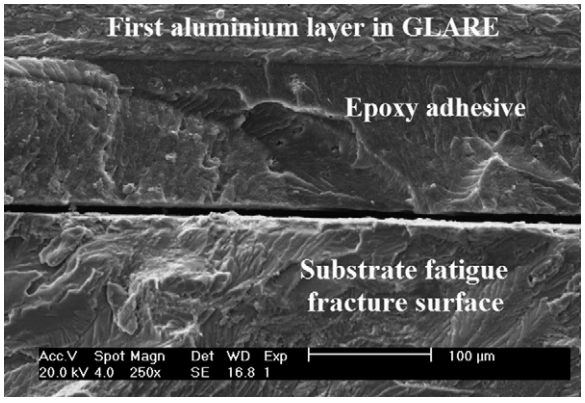

Fig. 17. SEM micrograph showing the fatigue fracture surface in the substrate and minor delamination between the 7085 substrate and the FM 94 adhesive.

almost all converted to deformation, internal damage and cracking. Lower frequency oscillations observed on the load—time traces in this work are mainly derived from dynamic resonances and vibrations. For the specimens studied here, obvious load drops did not occur. Rather for each impact energy tested only minor drops were observed. They could not be distinguished from the dynamic oscillations. It was observed in the sectioning and microscopy studies that fibre failure and matrix cracking occurred after impact. Any loading discontinuities associated with their formation may have been obscured by the size of the transient oscillations. The contact period of (1.5 ms) of each impact was found to be in agreement with that observed in tests on similar laminates, such as ARALL [18,19], carbon fibre and GLARE 3-2/1 [37], when impacted in the range 1.7–52 J. The maximum force obtained here was greater than previously observed by a factor two. This may be a consequence of the large (5 mm) thickness and consequent rigidity of the substrate.

It is important to note that C-scanning studies (Fig. 9) show that damage was formed even after 10 and 20 J impacts and that the internal damage extended further than the size of the visible dent (Table 3). Similar behaviour was observed by Wu in testing GLARE 5-2/1 and GLARE 4-3/2 laminates when directly impacted in the range 7–40 J [31] and after chemically removing the outer aluminium layers. In this research, significant delaminations between the non-impacted aluminium layer and the glass layer, together with a plastic deformation around the point of the impact, were observed. In addition, cracking of the fibre and matrix were found. Fibre failure and matrix cracking were found after impact in all of the specimens tested in this study. Figs. 10–12 also reveal matrix cracking is not located directly beneath the impacted area, but instead started from the edges of the damage area. This behaviour is consistent with the observation in the typical polymer matrix composite when impacted at a low velocity [38–40].

4.2. Fatigue behaviour

The application of the thin strap of GLARE 1-3/2 shows benefit to fatigue life and to crack propagation resistance of up to a factor of 5. Similar behaviour was found by Heinimann et al. [23] in testing 2.29 mm thick 6013-T6 and 6.35 mm 7085-T7651 panels reinforced with such laminate, and by Zhang et al. [25–27] in fatiguing 7085-T7651 reinforced with a variety of bonded straps. There are a number of reasons for this behaviour. There is modification of the local substrate stress due to the strap taking some of the applied load away from the substrate. In addition, the presence of the strap reduces the effective stress intensity factor at the crack tip due to the bridging effect when the crack propagates through and past the strap. The stiffness and geometry of both the strap and the substrate, i.e. stiffness ratio also affects the fatigue behaviour [22], and these parameters produce a reduction of the growth rate when the crack tip is under and beyond the strap. When the crack tip first encounters the strap edge and propagates under it, a delamination develops at the interface between the strap and the substrate, thus reducing the stiffness ratio and effectiveness of crack bridging. Therefore delamination crack growth will gradually reduce effectiveness of the strap. The adhesive cure temperature cycle is responsible for creation of tensile residual stresses in the substrate [25–27]; these will counter the beneficial effects of the strap [25,26,41]. In the case of this work it was observed that the major delamination occurred within the GLARE rather than between the outer layer of the GLARE and the substrate, the outer aluminium layer of the GLARE being severed via fatigue crack growth.

Introduction of impact damage in GLARE due to substrate impact caused a reduction in fatigue life and increased crack growth rate. These effects are believed to be because the strap stiffness will be reduced by the fractured glass fibres. The sample stiffness ratio will hence also be reduced. In addition, the impacted strap could have produced an increased stress intensity factor via reduced load transfer from the substrate to the strap [42], caused again by a reduction in the GLARE stiffness.

All the specimens tested in fatigue showed the same trend failure mode behaviour. In particular, the substrate crack cut through the FM94 adhesive and the outer aluminium layer of GLARE as a *Mode I* fatigue crack, the major delamination developing at the first glass fibre/epoxy layer of GLARE. A secondary delamination could be seen at the substrate/ FM94 interface as shown in Fig. 17, but this did not cause the failure of the strap and was evidently propagating slower than the delamination within the GLARE.

Delamination occurring on the latter interface could explain the fluctuations found in the measured fatigue crack growth rates. As other GLARE interfaces do not contribute to the delamination process, the crack bridging process occurring when the crack tip is beyond the strap was controlled in part by the properties of the first aluminium/glass fibre interface, as well as by strap stiffness. Increasing the delamination resistance of any other interface will not improve retardation behaviour further.

5. Conclusions

1. Impacts on the aluminium substrate of bonded GLARE aluminium hybrids with energies between 10 and 50 J, results in significant internal damage to both glass layers in the GLARE. The damage consists of fibre fractures splintering and matrix cracking.

2. No delamination between the substrate and GLARE was detected after impact, even at the highest energy levels. There was none at the interface between the aluminium and adhesive within the GLARE. Damage to the GRP could be detected even at the smallest impact energy of 10 J.
3. In fatiguing unimpacted bonded GLARE reductions in crack growth rate up to a factor of 5 were observed. After the impact, the retardation effect was a factor of 2.

Acknowledgements

Thanks are due to the Italian Air Force for making financially possible the attending of the MSc Advanced Materials at the Cranfield University (UK), Alcoa for AA 7085 and GTM for the GLARE.

References

[1] Committee on Aging of US Airforce Aircraft, Aging of US aircraft, National Materials Advisory Board, Publication NMAB-488-2, National Academy Press, Washington, DC, 1997.
[2] L.B. Vogelesang, A. Vlot, J. Mater. Process. Tech. 103 (2000) 1–5.
[3] R.C. Alderliesten, M. Hogenbeek, J.J. Homan, P.A. Hooijmeijer, T.J. de Vries, C.A.J.R. Vermeeren, Appl. Comp. Mater. 10 (2003) 223–242.
[4] E.C. Cleary, R.A. Dolbeer, S.E. Wright, Serial Report No. 9, Federal Aviation Administration, Office of Airport Safety Standard, Washington, DC, 2003.
[5] J. Lin, S. Ganguly, L. Edwards, P.E. Irving, Engineering Integrity Society: Proceedings of Fatigue 2003 Fatigue and Durability Assessment of Materials Components and Structures, Sheffield, UK, 2003, p. 65.
[6] Code of Federal Regulations, Aeronautics and Space, Part 25, Airworthiness Standard: Transport Category Airplanes.
[7] Joint Aviation Requirements, JAR-25, Large Aeroplanes; Global Engineering Documents, on behalf of Joint Airworthiness Authorities Committees.
[8] Z. Domazet, Eng. Fail. Anal. 3 (2) (1996) 137–147.
[9] B.J. Sutherland, F-111 Structural Integrity Assessment; addressing RAAF concerns, Sacramento Air Logistics Centre (MMKR) 82-1, Status Report, Sacramento Air Logistic Center, 1993.
[10] A.A. Baker, R. Jones, Bonded Repair of Aircraft Structures, Martinus Nijhoff, 1988.
[11] A. Vlot, J.M.A. Massar, C.B. Giujt, S. Verhoeven, Fatigue Fract. Eng. Mater. Struct. 23 (2000) 9–18.
[12] R.C. Alderliesten, J.J. Homan, Int. J. Fatigue 28 (10) (2006) 1116–1123.
[13] J.F. Lalibertè, C. Poon, P.V. Straznicky, A. Fahr, Polym. Compos. 21 (4) (2000) 558–567.
[14] X.R. Wu, Y.J. Guo, Fatigue Fract. Eng. Mater. Struct. 25 (2002) 911–922.
[15] H.M. Plokker, R.C. Alderliesten, R. Benedictus, Fatigue Fract. Eng. Mater. Struct. 30 (2007) 608–620.
[16] Y.J. Guo, X.R. Wu, Chin. J. Aer. 11 (1998) 152–156.
[17] A. Vlot, Composites Eng. 3 (10) (1993) 911–926.
[18] A. Vlot, Int. J. Impact Eng. 18 (3) (1996) 291–307.
[19] A. Vlot, E. Kroon, G. La Rocca, Key Eng. Mater. 141 (143) (1998) 235–276.
[20] R.C. Alderleisten, M. Hagenbeek, J.J. Homan, P.A. Hooijmeijer, T.J. De Vries, J.R. Vermeeren, Appl. Composites Mater. 10 (2003) 223–242.
[21] P.E. Irving, D. Figueroa, in: R. Benedictus, J. Schijve, R.C. Alderleisten, J.J. Homan (Eds.), First International Conference on Damage Tolerance of Aircraft Structures, ©TU Delft, The Netherlands, 2007.
[22] J. Schijve, Eng. Fract. Mech. 37 (1990) 405–421.
[23] M.B. Heinimann, R.J. Bucci, M. Kulak, M. Garrat, 23rd Symposium of the International Committee on Aeronautical Fatigue, ICAF 2005, vol. 1, Hamburg, June 2005, pp. 197–208.
[24] M.B. Heinimann, M. Kulak, R.J. Bucci, J. James, G. Wilson, J. Brokenbrough, H. Zonker, H. Skyut, Proceedings 24th Symposium of the International Committee on Aeronautical Fatigue, Naples, May 2007.
[25] X. Zhang, D. Figueroa, M. Boscolo, G. Allegri, P.E. Irving, Proceedings 24th Symposium of the International Committee on Aeronautical Fatigue, Naples, May 2007.
[26] X. Zhang, M. Boscolo, D. Figueroa, G. Allegri, P.E. Irving, Eng. Fract. Mech. 76 (2009) 114–133.
[27] M. Boscolo, X. Zhang, G. Allegri, 48th AIAA/ASME/ASCE/AHS/ASC Structures Structural Dynamics and Materials Conference, AIAA, 2007, pp. 2007–2116.
[28] W.S. Johnson, NASA TM-89013, 1986.
[29] J.F. Lalibertè, C. Poon, P.V. Straznicky, A. Fahr, Int. J. Fatigue 24 (2002) 249–256.
[30] G. Wu, J.M. Yang, T.H. Hahn, J. Mater. Sci. 42 (2007) 948–957.
[31] G. Wu, J.M. Yang, J. Miner. Met. Mater. Soc. 57 (1) (2005) 72–79.
[32] F. Bagnoli, MSc thesis, Cranfield University (UK), 2006.
[33] Cytec data sheet FM 94, Cytec Engineering Materials; http://www.cytec.com/engineered-materials/products/datasheets/FM94.pdf.
[34] D.D.R. Cartiè, P.E. Irving, Composites Part A 33 (2002) 483–493.
[35] G. Caprino, G. Spataro, S. Del Luongo, Composites Part A 35 (2004) 605–616.
[36] G.D. Lawcock, L. Ye, Y.W. Mai, C.T. Sun, Compos. Sci. Tech. 57 (1997) 1621–1628.
[37] J.F. Lalibertè, P.V. Straznicky, C. Poon, Am. Inst. Aeronaut. Astronaut. 43 (11) (2005) 2445–2453.
[38] H.Y. Choi, H.Y.T. Wu, F.K. Chang, J. Compos. Mater. 25 (1991) 992.
[39] S.P. Joshi, C.T. Sun, J. Compos. Mater. 19 (1985) 51.
[40] D. Liu, L.E. Malvern, J. Compos. Mater. 21 (1987) 594.
[41] M. Colavita, A. Bowler, X. Zhang, P.E. Irving, Proceedings of SAMPE 2006, Long Beach, April 30–May 4 2006, CA, USA, 2006.
[42] R. Rodi, R. Alderliesten, R. Benedictus, Proceedings 24th Symposium of the International Committee on Aeronautical Fatigue, Naples, May 2007.